Analysis of hydrodynamic journal bearings considering lubricant supply conditions

J C P Claro and **A A S Miranda**, MSc, PhD
University of Minho, Guimarães, Portugal

A method of analysis of steadily loaded hydrodynamic journal bearings with a single axial groove (either on the load line or at 90° to the load line) or two diametrically opposed axial grooves is described. The method is based on Elrod's cavitation algorithm (which ensures conservation of mass flow in both the full film and the cavitated regions) and is able to accommodate specified lubricant supply conditions, namely groove size and location and supply pressure. Special attention has been given to the determination of flowrate.

The equation governing the distribution of pressure around the bearing has been solved numerically using a finite differences approximation and multi-grid techniques to accelerate the convergence of the solution. Performance predictions of the analysis are compared with published experimental data and with experimental measurements obtained in laboratory tests carried out by the authors. The data used cover all grooving arrangements studied.

NOTATION

a	groove dimension in axial (y) direction
b	bearing width
c_d	diametral clearance
d	nominal diameter
g	cavitation index
h	film thickness
H	power loss
m	mass flow per unit width
M	circumferential number of grid points
n	shaft speed of rotation
N	axial number of grid points
p	pressure
P_x	pressure force component perpendicular to the line of centres
P_z	pressure force component along the line of centres
Q	lubricant flowrate
RF	relaxation factor in Gauss–Seidel iteration
U	tangential speed of the shaft surface
w	groove dimension in circumferential (x) direction
W	load capacity
x	circumferential coordinate
y	axial coordinate
β	bulk modulus of the lubricant
ε	eccentricity ratio
Θ	Elrod's variable
μ	absolute viscosity of the lubricant
ρ	density of the lubricant
ϕ	attitude angle

Subscripts

av	average
c	cavitation
f	supply
i	points on the circumferential mesh line (i)
j	points on the axial mesh line (j)
max	maximum value
p	pressure
v	velocity

The MS was received on 10 August 1992 and was accepted for publication on 18 February 1993.

x	circumferential direction
y	axial direction

Dimensionless parameters

$\bar{h}$	dimensionless film thickness $= 2h/c_d$
$\bar{H}$	power loss parameter $= H \dfrac{c_d}{\mu U^2 bd}$
$\bar{p}_f$	supply pressure parameter $= p_f \dfrac{(c_d/d)^2 d/2}{\mu U}$
$\bar{Q}$	flowrate parameter $= \dfrac{Q}{Ubc_d/2}$
$\bar{W}$	load capacity parameter $= W \dfrac{(c_d/d)^2}{\mu U b}$
$\bar{x}$	dimensionless circumferential coordinate $= x/(\pi d)$
$\bar{y}$	dimensionless axial coordinate $= y/b$
$\bar{\beta}$	bulk modulus parameter $= \beta \dfrac{(c_d/d)^2 d/2}{\mu U}$

1 INTRODUCTION

Hydrodynamic journal bearings are commonly used for supporting rotating shafts subjected to high static radial loads. Applications can be seen in a wide variety of machines where satisfactory performance is vital for proper functioning, such as pumps, turbines, compressors, gear boxes, etc.

The ability of design engineers to predict with confidence and precision important operating characteristics of such bearings is not good. One of the features limiting this ability is the poor estimation of lubricant flowrate, as shown by McCallion *et al.* (1), Etsion and Pinkus (2), Basri and Neal (3), among others.

Improving the accuracy of flow determination becomes relevant in design when looking for high overall efficiency. The present tendency is to reduce the number of shaft supports and their width, seeking a full utilization of each bearing, which means to take its operating eccentricity from the usual value of 0.7–0.8 to

0954-4062/93 $3.00 + .05

the 0.8–0.9 range. As flowrate highly influences the lubricant temperature and viscosity and this, in turn, determines the load capacity and the eccentricity, an error in the determination of the first is necessarily reflected in the prediction of the last. Thus, a deficient design can become not just a question of operating parameters different from those expected, but a serious possibility of damaging the component.

Widely used procedures for the design of steadily loaded journal bearings, such as ESDU 84031 (**4**), have adopted a lubricant flow analysis based on Barnard's work (**5**), assuming that the total flow is the sum of a velocity flow component (Q_v) due to the movement of the shaft and a pressure flow component (Q_p) due to the lubricant supply pressure. Additionally the oil is assumed to be totally expelled and renewed by fresh oil entering the groove, after having travelled 360° around the bearing.

Besides the inaccuracy that such a superimposition of contributions can introduce due to flow discontinuity in the analytical simulation, other questions are not considered in this approach, namely the real geometry and location of the reformation boundary and the possibility of incomplete renewal of the oil, implying a certain amount of recirculation. In this matter, several experimental published results (**6–8**) have shown that important discrepancies between theoretical predictions and experimental observations can be found.

Elrod and Adams (**9**) have proposed an algorithm, later refined by Elrod (**10**), that automatically takes into account the occurrence of cavitation, ensuring mass flow continuity within both the full film and the cavitation region, and across cavitation and reformation boundaries. Implementations of the method have already been carried out by Dowson *et al.* (**11**) for journal bearings with one axial groove at h_{max}, Clayton and Taylor (**12**) for circumferentially grooved bearings and Brewe (**13**) and Woods (**14**) for the dynamically loaded hydrodynamic journal bearing.

In the present paper a method of analysis of steadily loaded journal bearings with a single axial groove, either on the load line or at 90° to the load line, and two diametrically opposed axial grooves (Fig. 1) is described. The method is based on Elrod's algorithm and accepts lubricant supply conditions (namely groove size and location and supply pressure) as entry parameters. Theoretical predictions are compared with experimental data available.

This is part of a broader project aimed at the production of a matrix of theoretical results for a wide range of variation of geometric and operating parameters (such as ε, b/d, $\bar{p}_f$, a/b) and their validation by experiments. The results obtained allowed the construction of the design charts for load capacity, flowrate and power loss, for those bearing types. This will be the subject of a future paper.

2 THEORETICAL ANALYSIS

2.1 Implementation of Elrod's method

The equation governing the generation of hydrodynamic pressure in the continuous film region of the bearing is Reynolds' equation, which for an incompressible isoviscous lubricant and steady state operating conditions takes the form:

$$\frac{\partial}{\partial x}\left[h^3 \frac{\partial p}{\partial x}\right] + \frac{\partial}{\partial y}\left[h^3 \frac{\partial p}{\partial y}\right] = 6\mu U \frac{\partial h}{\partial x} \tag{1}$$

Elrod (**10**) has proposed an algorithm for the solution of equation (1) which allows its application all around the bearing and automatically locates the cavitated region without explicit reference to rupture or reformation boundary conditions. Mass flow continuity is ensured all around the bearing by changing the form of equation (1), introducing a new variable (Θ) and a cavitation index (g).

The variable Θ had two distinct meanings:

1. In the continuous film region (where $p \geqslant p_c$), the change of density (ρ) with pressure leads to the definition of Θ as ρ/ρ_c or, based on the definition of bulk modulus (β),

$$\Theta = \frac{p - p_c}{\beta} + 1 \tag{2}$$

2. In the cavitated region (where $p = p_c$), the mass flow per unit width of film equals $\Theta \rho_c h$, Θ being the fraction of the bearing width occupied by the oil strips, dragged by shaft rotation.

Therefore,

$$\Theta \begin{cases} < 1 & \text{for } p = p_c \quad \text{(cavitation region)} \\ \geqslant 1 & \text{for } p > p_c \quad \text{(full film region)} \end{cases} \tag{3}$$

Additionally, a cavitation index (g) was defined as

$$g = \begin{cases} 0 & \text{when } \Theta < 1 \\ 1 & \text{when } \Theta \geqslant 1 \end{cases} \tag{4}$$

A finite differences mesh was considered over half the developed bearing area, as only the case of a well-aligned bearing was considered. Figure 2 shows the

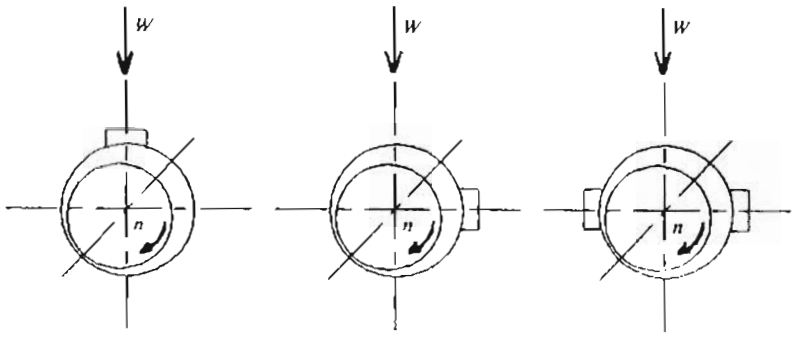

Fig. 1 Grooving arrangements covered by the present analysis

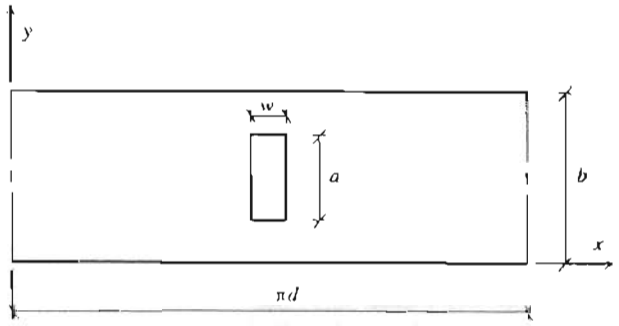

Fig. 2 Developed bearing surface showing the coordinate axis and bearing and groove geometry

'unwrapped' bearing surface and on Fig. 3 a point (i, j) and the corresponding computational cell are represented. The number of axial and circumferential mesh points was N and M respectively.

The mass flow entering the cell in a given direction (say, the x direction) is the sum of Couette and Poiseuille components, given by

$$(\dot{m}_x)_C = \frac{\rho_c U}{2}\left\{\Theta_{i,j-1}h_{j-1}(1-g_{i,j-1}) + g_{i,j-1}h_{j-1} + \frac{g_{i,j-1}g_{i,j}}{2}(h_j - h_{j-1})\right\}$$

$$(\dot{m}_x)_P = \frac{h_{av}^3}{12\mu}\beta\rho_c\left\{\frac{g_{i,j-1}(\Theta_{i,j-1}-1) - g_{i,j}(\Theta_{i,j}-1)}{\Delta x}\right\}$$

Mass flow balance applied to the cell takes the following form:

$$(\Delta\dot{m}_x)\,\Delta y + (\Delta\dot{m}_y)\,\Delta x = 0 \tag{5}$$

where $\Delta\dot{m}_x$ and $\Delta\dot{m}_y$ are the net mass flows per unit width entering the cell in the x and y directions.

The application of equation (5) at each point (i, j) allowed the construction of a system of linear equations in Θ:

$$\Theta_{i,j} = \frac{\Delta\bar{x}\bar{\beta}\pi/24(d/b)^2 Y_3 + \Delta\bar{y} \times \frac{1}{2} \times X_8 + \Delta\bar{y}\bar{\beta}/(96 \times 2\pi)X_7}{\Delta\bar{x}\bar{\beta}\pi/24(d/b)^2 Y_1 + \Delta\bar{y} \times \frac{1}{2} \times X_1 + \Delta\bar{y}\bar{\beta}/(96 \times 2\pi)X_3} \tag{6}$$

The parameters involved in equation (6) are defined in the Appendix.

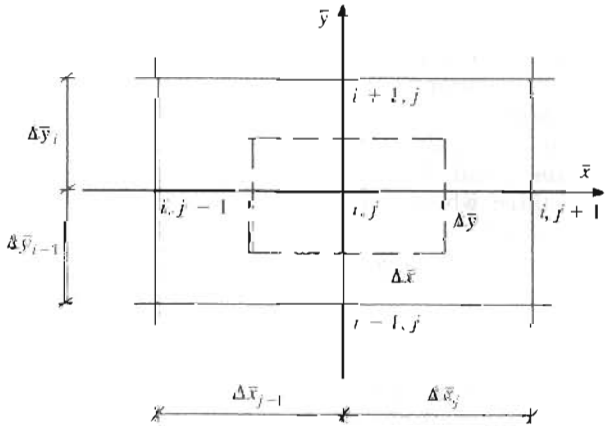

Fig. 3 Point (i, j) and the corresponding computational cell

2.2 Solution of the finite differences equation

The solution of the system of equations (6) allowed the determination of Θ at each point and, therefore, the pressure distribution, according to equations (2) and (3). A Gauss–Seidel iterative method was used. Initially, Θ values were set to zero and g values to unity.

Boundary conditions were imposed assuming ambient pressure along the bearing edges and a value of pressure equal to the supply pressure over the groove(s). The corresponding values of Θ were calculated according to equation (2). Cavitation pressure was assumed to be the ambient pressure.

After each iteration the starting values of Θ at every point for a new iteration (k) were given by

$$\Theta^{(k)} = \Theta^{(k-1)} + \mathrm{RF}(\Theta^{(c)} - \Theta^{(k-1)}) \tag{7}$$

where

RF = relaxation factor

$k - 1$ = previous iteration

$\Theta^{(c)}$ = calculated value in the iteration k, using equation (6)

The following criteria for convergence were used:

(a) stability of the g values at all points:

$$g_{i,j}^{(k)} = g_{i,j}^{(k-1)}$$

(b) variation of the mean value of Θ:

$$\sum_{j=1}^{M}\sum_{i=1}^{N}\frac{(\Theta_{i,j}^{(k)} - \Theta_{i,j}^{(k-1)})/\Theta_{i,j}^{(k-1)}}{MN} < \text{tolerance} \tag{8}$$

Two other parameters were found to be relevant to the process:

1. The relaxation factor (RF), which was usually set to unity. The use of values smaller than unity caused problems of convergence. The influence of RF on the number of cycles for convergence of the solution is shown in Fig. 4a.
2. The bulk modulus (β), the value of which did not affect the final solution, had, however, a significant influence on the processing time. This is shown in Fig. 4b. The value of the bulk modulus parameter $(\bar{\beta})$ adopted was 0.01, because problems of convergence arose for values in the range 0.02–0.10.

2.3 Grid generation and mesh size

As precision in flow determination is directly dependent on the geometry and location of the cavitation and reformation boundaries, a refinement of the mesh in those regions was convenient. However, due to the wide variety of parameters used, an estimation of the extent of the region where the mesh should be refined was sometimes difficult to make with some degree of confidence. It was therefore decided to use a multi-grid technique, starting with a grid of constant mesh size in the circumferential direction and then generating automatically two other grids, as follows:

(a) initial grid (Fig. 5a), with a constant circumferential mesh size and a relatively small number of points;
(b) fine grid (Fig. 5b), based on the initial grid, with the number of circumferential points doubled in the region of a continuous film;

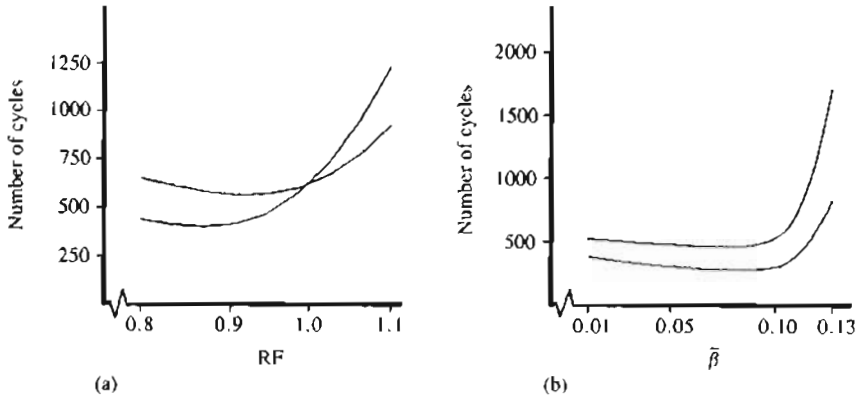

Fig. 4 Influence on the number of cycles for convergence of the RF and $\bar{\beta}$ for two sets of operating conditions

(c) coarse grid (Fig. 5c), generated from the fine grid, by elimination of even points both axially and circumferentially.

During the convergence process the mean variation of Θ in successive iterations decreases as the solution is approached. The mean variation of Θ at a given stage of the iterative process was taken as a measure of 'speed' of convergence at that stage of the process. The iterative process was run over the initial grid until the mean variation of Θ between cycles stayed below 10^{-2}, which corresponded to about 5 per cent of the total number of iterations needed to final convergence, and that experience was shown to correspond to a stage where the position of both boundaries was defined within two circumferential mesh points.

The fine grid was then generated. From the (less precise) solution previously obtained the points belonging to the boundaries were identified and the value of Θ for the new points created in the continuous film region was calculated by quadratic interpolation over the previously existent points in the neighbourhood. This fine grid was used until the speed of convergence dropped to a pre-set value. Then Θ values were directly passed on to the coarse grid to continue the iterative process. The same analysis of the variation of Θ in successive iterations was taken once again to return to the fine grid, over which final convergence was reached.

A study was undertaken in order to determine the most suitable strategy for speed of convergence, in terms of number of cycles and in processing time, as iterative cycles over the coarse grid were considerably quicker but their convergence to a smaller tolerance had no effect on time saved over the subsequent fine grid. Although operating parameters might also influence the best choice, it was found that a significant overall improvement could be achieved with the following values of 'speed', corresponding to the allowed minimum mean variation of Θ in each grid:

10^{-02} = change from initial to fine grid

10^{+10} = change from fine to coarse grid

10^{-04} = change from coarse to fine grid (final)

Considerable improvements were noticed both in number of cycles and processing time, as can be seen in Tables 1 and 2. However, the main advantage of this technique was found to be the possibility of getting the solution of a considerable number of cases (especially those at high values of the supply pressure parameter) which would not have converged in the single grid approach. Examples of such cases are marked (*) in Tables 1 and 2.

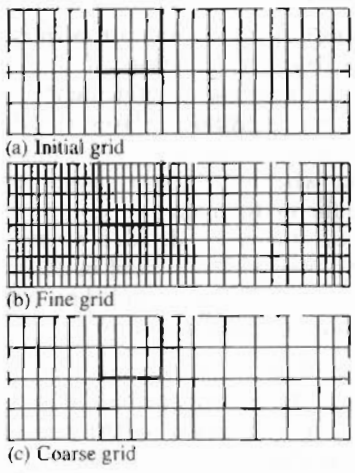

Fig. 5 A sketch of the automatic process of grid generation

2.4 Bearing performance

The program accepted as input parameters the eccentricity ratio (ε), the dimensionless supply pressure ($\bar{p}_f$) and the geometric parameters b/d, a/b and w/d, referring to the bearing width and the groove dimensions. After convergence was reached in Θ the determination of the pressure distribution allowed the calculation of the performance parameters. Numerical integrations were performed using Simpson's rule.

The pressure gradient at a given point in a given direction was calculated assuming that the pressure variation could be represented by a polynomial of degree three whose coefficients were determined from the knowledge of the pressure values at four successive points in that direction.

2.4.1 Load capacity

This was calculated by axial and circumferential integration of the hydrodynamic pressure distribution and subsequent vectorial addition of these components in

Table 1 Number of cycles and CPU time for convergence for the case of one axial groove at $+90°$ to the load line ($b/d = 0.5$, $a/b = 0.5$, $w/d = 0.2$)

Eccentricity ratio ε	$\bar{p}_f = 0$				$\bar{p}_f = 0.5$			
	Multi-grid		Single-grid		Multi-grid		Single-grid	
	cycles	s	cycles	s	cycles	s	cycles	s
0.3	743	1047	1417	1193	471	676	748	1037
0.5	264	270	808	965	255	963	*	*
0.7	212	218	819	960	230	253	562	678
0.9	189	188	762	912	182	185	223	261

two directions. The expressions used were

$$\bar{P}_x = 2\pi \int_0^1 \int_0^1 (\bar{p} \sin \alpha)\, d\bar{x}\, d\bar{y}$$

$$\bar{P}_z = -2\pi \int_0^1 \int_0^1 (\bar{p} \cos \alpha)\, d\bar{x}\, d\bar{y} \qquad (9)$$

$$\bar{W} = (\bar{P}_x^2 + \bar{P}_z^2)^{1/2}$$

2.4.2 *Flowrate*

The expressions used to determine flowrate in the circumferential and axial directions were

$$\bar{Q}_x = \int_0^1 \left(-\frac{\bar{h}^3}{24\pi} \frac{\partial \bar{p}}{\partial \bar{x}} + \frac{\bar{h}}{2} \right) d\bar{y} \qquad (10)$$

$$\bar{Q}_y = \pi \left(\frac{d}{b}\right)^2 \int_0^1 \left(-\frac{\bar{h}^3}{24} \frac{\partial \bar{p}}{\partial \bar{y}} \right) d\bar{x} \qquad (11)$$

The precision of the solution was assessed by comparison of the values of flowrate determined in two different ways (**11**):

1. Flow (out) from the bearing sides.
2. Flow issuing from the supply groove(s). This calculation involved the identification of the different existing boundaries and their location in relation to the grooves. Several situations may be expected which involve the determination of flowrate on a pressure gradient basis in the continuous film region or directly from the values of Θ in the cavitated region. All the situations that can occur were incorporated in the analysis and are shown in Fig. 6.

Since alternative 1 is mainly dependent on the circumferential number of points and alternative 2 on the axial number of points, the difference between these two values of flowrate was taken as a measure of the suitability of the M/N ratio used.

2.4.3 *Power loss*

The following expression was used to calculate the dimensionless power loss:

$$\bar{H} = \int_0^1 \int_0^1 \left[\frac{2\pi}{\bar{h}} + \frac{\bar{h}}{2} \frac{\partial \bar{p}}{\partial \bar{x}} \right] d\bar{y}\, d\bar{x} \qquad (12)$$

2.4.4 *Attitude angle*

Film thickness at every point was calculated with reference to the line of centres, as well as the location of the groove(s). After each converged iteration on pressures the determination of the load components (and, therefore, of the attitude angle) might or might not confirm the initial position assumed for the line of centres.

Therefore the iterative process to determine the pressure distribution was inside another iteration to calculate the correct value of attitude angle (Φ). The starting value of Φ for a given ε was determined by polynomial interpolation over curves for the variable $\bar{p}_f$, obtained for fixed values of the geometric parameters ($b/d = 0.5$, $a/b = 0.5$, $w/d = 0.2$).

At the end of each iteration on pressures the attitude angle was calculated from

$$\Phi = \tan^{-1}\left(\frac{\bar{P}_x}{\bar{P}_z}\right) \qquad (13)$$

This value was checked against the previous one and the process was terminated if they were within a tolerance of $360°/M$. Otherwise a new value of Φ, which was the mean of the other two, was taken to start a new iterative process.

3 COMPARISON OF RESULTS

A comparison of theoretical results with experimental data available was carried out to assess the validity of the analysis. This comparison was mainly in terms of flowrate, but in two cases the predictions of power loss were also checked.

Table 2 Number of cycles and CPU time for convergence for the case of two axial grooves at $\pm 90°$ to the load line ($b/d = 0.5$, $a/b = 0.5$, $w/d = 0.2$)

Eccentricity ratio ε	$\bar{p}_f = 0$				$\bar{p}_f = 0.5$			
	Multi-grid		Single-grid		Multi-grid		Single-grid	
	cycles	s	cycles	s	cycles	s	cycles	s
0.3	364	412	*	*	500	617	811	1021
0.5	283	309	806	1020	281	346	813	1092
0.7	352	407	819	1042	326	352	*	*
0.9	214	222	768	1003	1017	1263	*	*

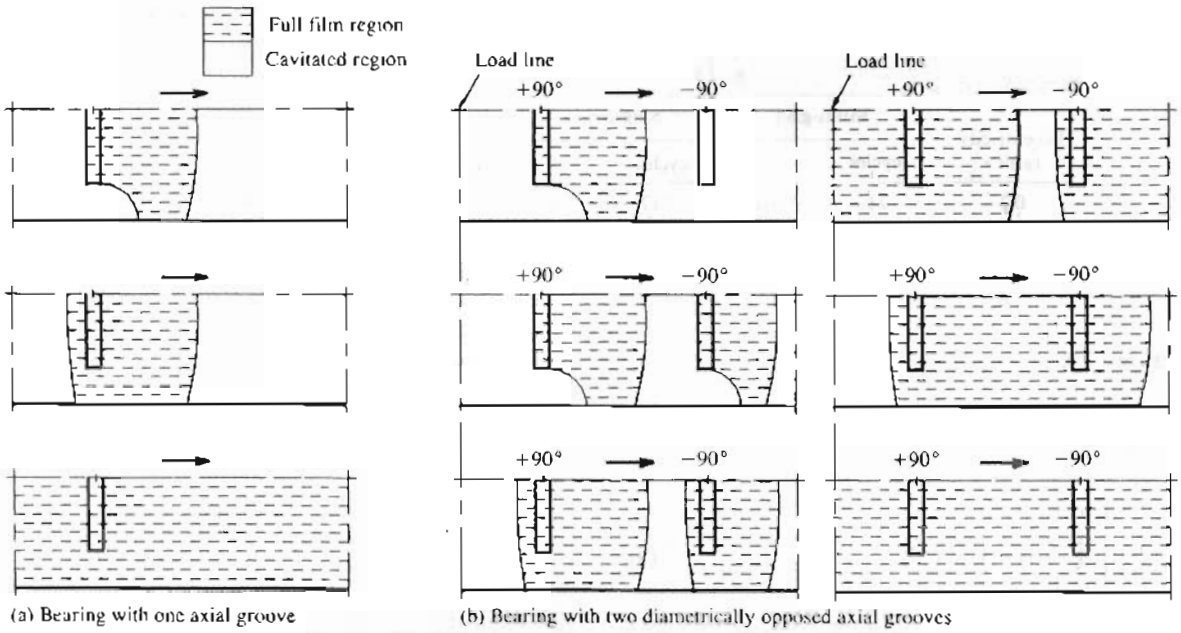

Fig. 6 A sketch of the full film/cavitated regions, which can be identified by the program prior to calculation of the flow of lubricant issuing from the grooves

Experimental results of Dowson *et al.* (7) and McKee (15) for bearings with one axial groove on the load line were used. For bearings with one and two grooves at right angles to the load line, published results were scarce and the few available for the latter case (16) could not be successfully simulated by the program.

An experimental apparatus was conceived and built, and a programme of tests covering a wide range of variation of parameters was carried out, to validate the theoretical analysis. A floating bronze bush was mounted on a 50 mm diameter shaft driven by a variable speed d.c. motor. The load was applied to the bush by flexible steel cables connected to a multiplying arm with dead-weights. The oil was pumped from an oil tank to the bearing by a constant speed screw pump. The supply pressure was measured in the supply groove by means of a pressure transducer and could be varied, actuating a flow valve on the oil circuit. Oil inlet and outlet temperatures were measured by K-type thermocouples. The oil flowrate was measured using a gear flowmeter mounted on the supply line. In operation, the displacement of the bush in relation to the shaft was evaluated using four contactless displacement transducers, two on each side of the bush, 90° apart. Bushes of different width, clearance and groove size were tested. This experimental work will be the subject of a future paper, but sample results are presented here.

Table 3 shows bearing geometries and operating conditions corresponding to the experimental results used for comparison. They were made non-dimensional according to the expressions adopted in the present work, using an oil viscosity corresponding to the measured outlet temperature.

Figures 7 and 8 show a comparison of experimental values of dimensionless flowrate with the predictions of the analysis, for bearings with a single axial groove on the load line. A comparison of dimensionless power loss is shown in Fig. 9. The operating conditions cover low and high values of a/b and $\bar{p}_f$ and values of ε ranging from 0.31 to 0.94. The correlation observed for both $\bar{Q}$ and $\bar{H}$ was good. Maximum discrepancies were of 17 per cent on flowrate and 10 per cent on power loss.

Table 3 Experimental bearing geometries and operating conditions

	Groove on the load line				Groove at +90° to the load line			Groove at ±90° to the load line		
	McKee (15)		Dowson (7)		Authors' experiments			Authors' experiments		
	Fig. 7a	Fig. 7b	Figs 8, 9a	Figs 8, 9b	Fig. 10a	Fig. 10b	Fig. 10c	Fig. 11a	Fig. 11b	Fig. 11c
d (mm)	52.3		101.6			50			50	
b/d	0.620		0.750			1.0			1.0	
a/b	0.098		0.875			0.8			0.8	
w/d	0.061		0.047			0.2			0.2	
c_d/d	0.0016	0.0025	0.0013			0.005			0.005	
W (N)	6900		Variable	8900	Variable	824	824	Variable	824	824
n (r/s)	33.8		25.0	Variable	8.6	8.6	Variable	8.5	8.5	Variable
p_s (kPa)	Variable		276		60	Variable	40	50	Variable	30
μ(Pl)										
40°C	0.0630		0.0225			0.0750			0.0750	
100°C	0.0081		0.0044			0.0089			0.0089	

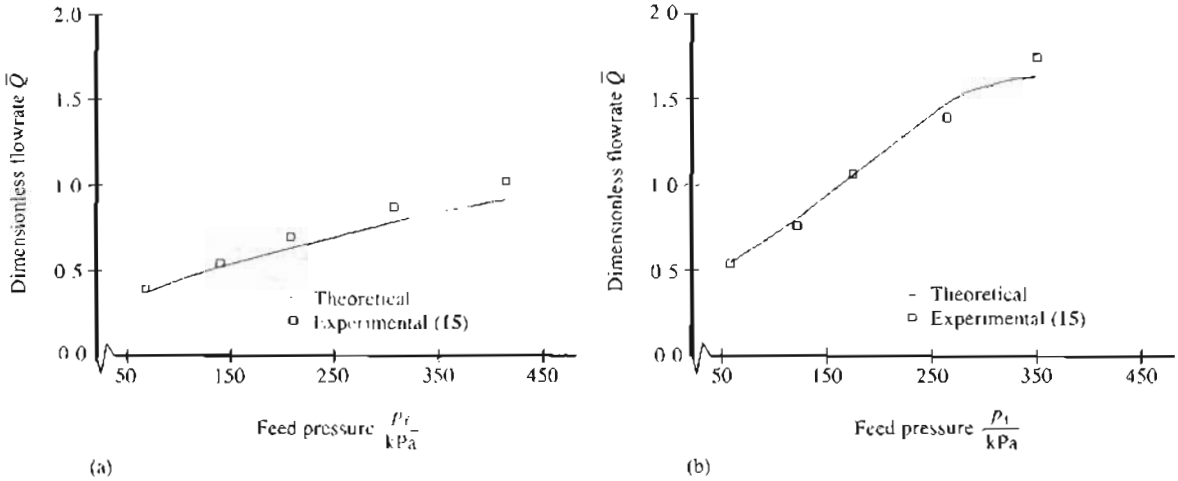

Fig. 7 Comparison of theoretical predictions of dimensionless flowrate with experimental results (15). (Calculated eccentricity ratios: (a) 0.90 and (b) 0.94)

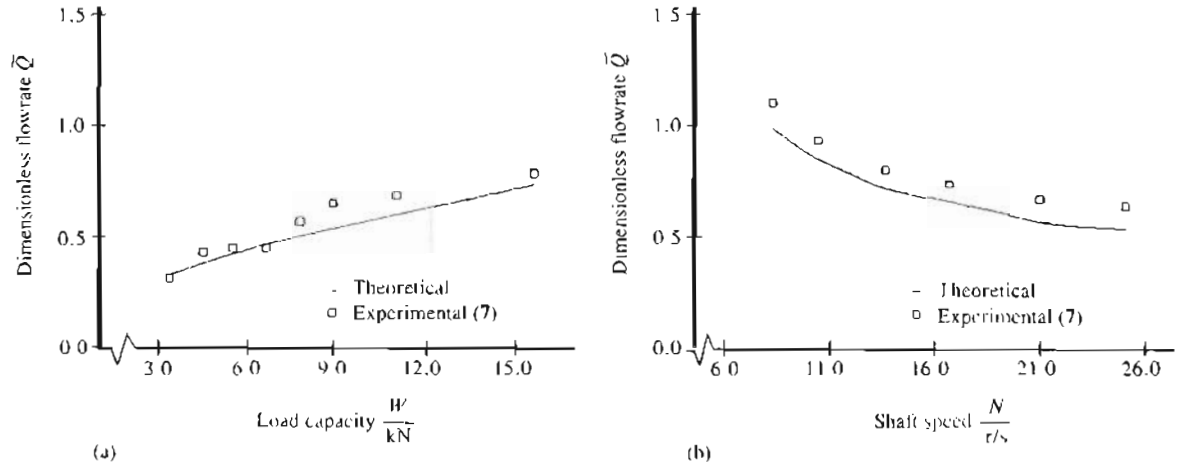

Fig. 8 Comparison of theoretical predictions of dimensionless flowrate with experimental results (7). (Calculated eccentricity ratios: (a) 0.31–0.64 and (b) 0.67–0.51)

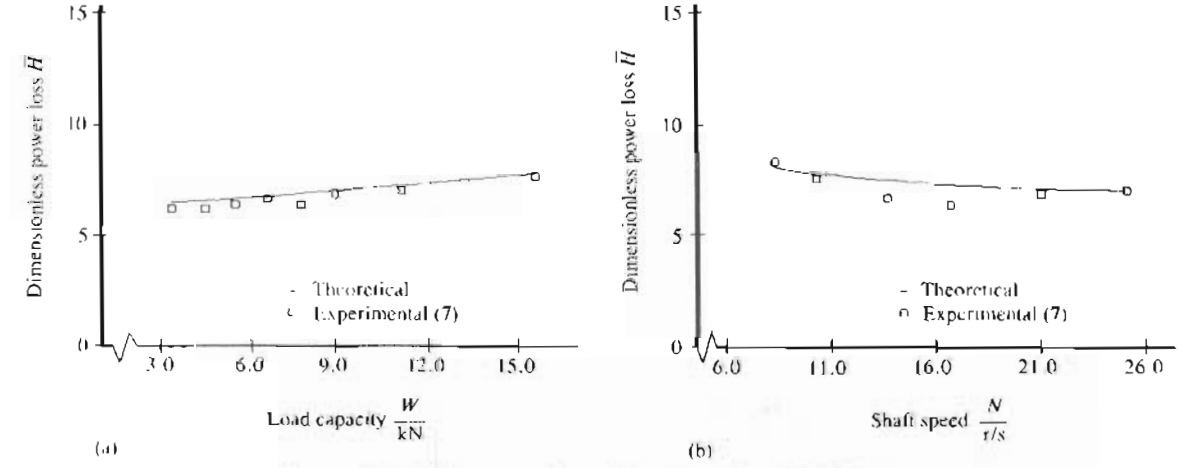

Fig. 9 Comparison of theoretical predictions of dimensionless power loss with experimental results (7). (Calculated eccentricity ratios: (a) 0.31–0.64 and (b) 0.67–0.51)

A comparison of experimental measurements of flowrate with theoretical predictions of the present analysis for journal bearings with one axial groove at 90° to the load line is shown in Fig. 10. Results were obtained for a given bearing geometry, varying the applied load, rotational speed and oil supply pressure. The correlation is acceptable and the results showed the same trend in all cases. Maximum discrepancies were of 28,

25 and 30 per cent in Fig. 10 for cases (a), (b) and (c) respectively. The corresponding mean discrepancies were of 22, 21 and 23 per cent. The predicted values of dimensionless flowrate were always higher than the values measured.

The predictions of ESDU 84031 (**4**), a commonly used procedure for the design of hydrodynamic journal bearings, have been worked out for all cases illustrated in Fig. 10. These predictions were always higher (sometimes significantly) than the predictions of the present analysis.

The theoretical predictions of dimensionless flowrate for bearings with two diametrically opposed axial grooves were also compared with experimental measurements. The bearing geometry was the same as for Fig. 10. The comparative results are shown in Fig. 11. Again the correlation is acceptable in all cases, the trends being the same for both theoretical and experi-

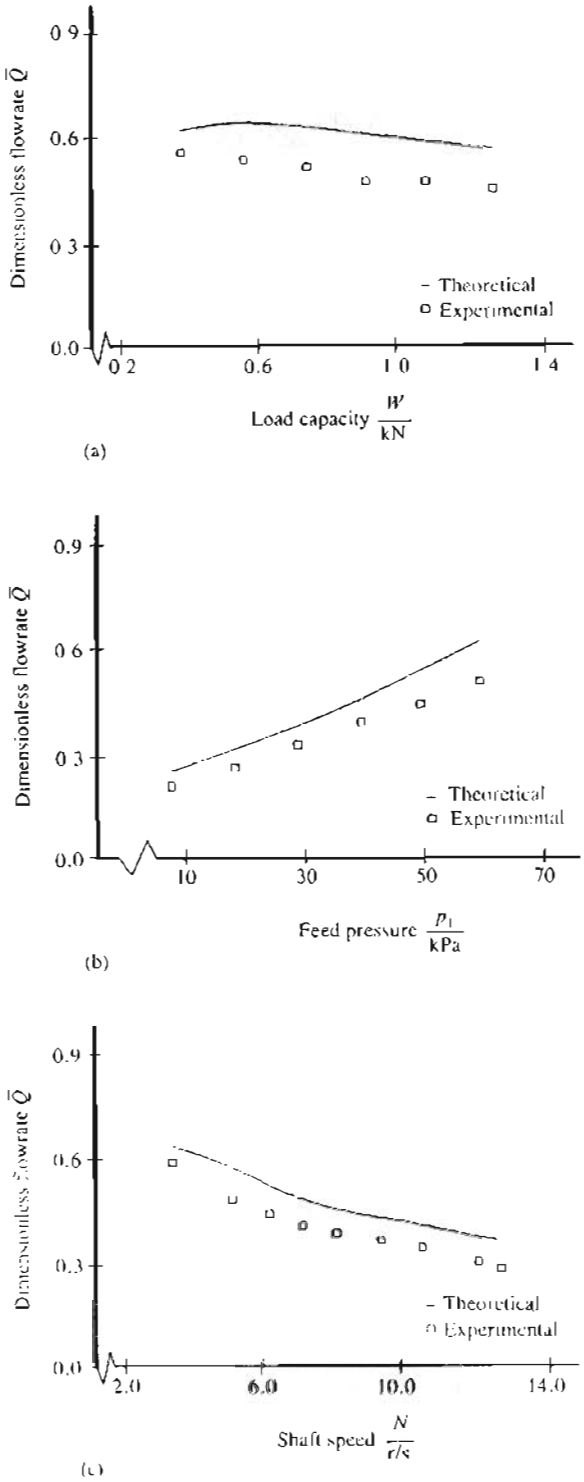

Fig. 10 Comparison of theoretical predictions of dimensionless flowrate with experimental results for one groove at $+90°$ to the load line. (Calculated eccentricity ratios: (a) 0.52–0.80, (b) 0.73 and (c) 0.84–0.62)

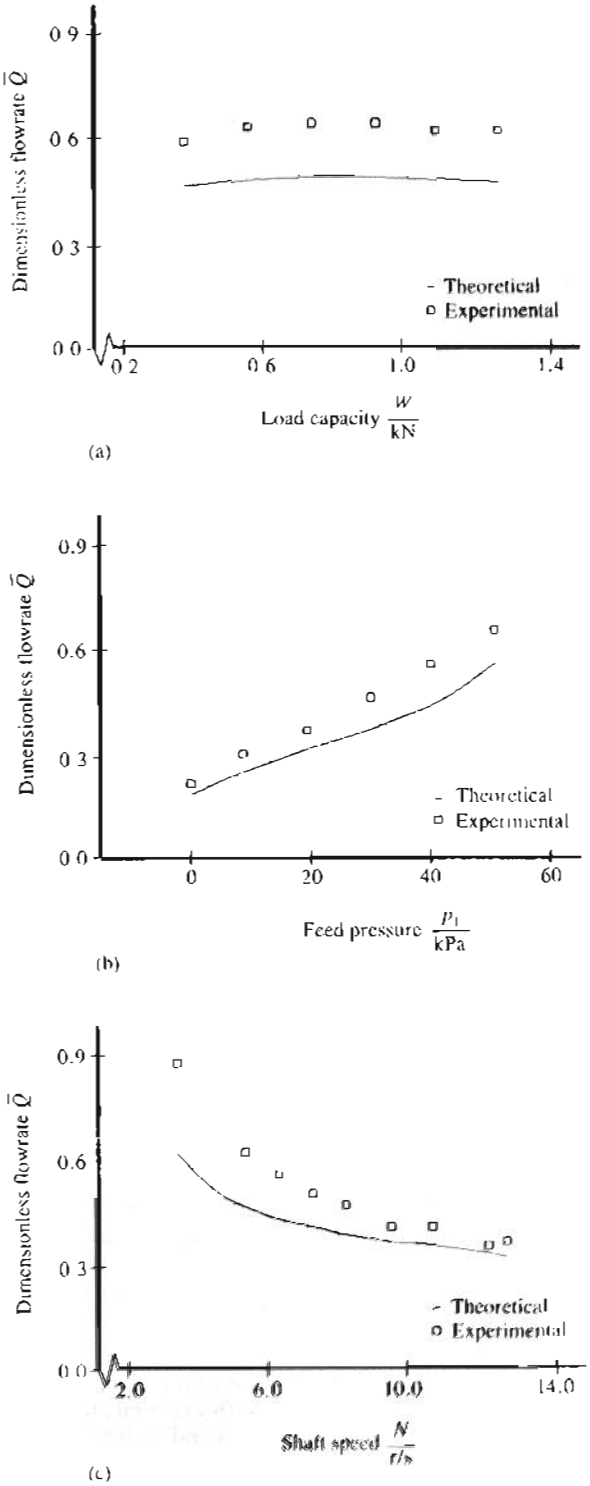

Fig. 11 Comparison of theoretical predictions of dimensionless flowrate with experimental results for two grooves at $\pm 90°$ to the load line. (Calculated eccentricity ratios: (a) 0.48–0.78, (b) 0.70 and (c) 0.83–0.61)

mental results. Maximum discrepancies found were of 24, 25 and 28 per cent for cases (a), (b) and (c) respectively. The corresponding mean discrepancies were of 23, 18 and 17 per cent. The predictions of flowrate were smaller than the measured flowrate in all cases. The worked-out predictions of ESDU 84031 (4) lay between the experimental values and the predictions of the present analysis.

4 CONCLUSIONS

1. A theoretical analysis developed by one of the authors (17) for steadily loaded hydrodynamic journal bearings with one axial groove at the maximum film thickness, based on Elrod's cavitation algorithm (10), has been improved and extended to bearings with a single axial groove (either on the load line or at 90° to the load line) and two diametrically opposed axial grooves. The method is able to accommodate variable groove geometry and location as well as variable lubricant supply pressure.
2. A multi-grid technique has been used which decreased the number of cycles for convergence of the numerical solution of the finite difference equations and allowed convergence for cases where it had not been possible with a single grid.
3. Predictions of the analysis for flowrate and power loss have been compared with experimental measurements of Dowson *et al.* (7), McKee (15) and the authors. The correlation observed was good for bearings with a single axial groove on the load line and not as good, but nevertheless acceptable, for the other grooving arrangements studied.

The work reported in this paper is only one part of a broader study which included a programme of laboratory tests for validation of the theoretical predictions. The results of this study allowed the construction of performance charts for all bearing types considered. This will be the subject of future papers.

ACKNOWLEDGEMENTS

This work was carried out with the financial support of JNICT (Portugal) under contract 87.70/MATR. The authors wish to thank Professor C. M. Taylor of Leeds University for his interest in the study and for discussions held at different stages of the work.

REFERENCES

1 **McCallion, H. M., Lloyd, T.** and **Yousif, F. B.** The influence of oil supply conditions on the film extent and oil flow in journal bearings. IMechE Tribology Convention, 1971, pp. 31–37 (Institution of Mechanical Engineers, London).
2 **Etsion, I.** and **Pinkus, O.** Solutions of finite journal bearings with incomplete films. *Trans. ASME*, 1975, **97**(1), 89–100.
3 **Basri, H.** and **Neal, P. B.** Oil flow in axial groove journal bearings. IMechE Tribology Group Seminar on *Developments in plain bearings for the '90s*, London, 17 May 1990, pp. 11–17 (Mechanical Engineering Publications, London).
4 ESDU 84031: 1984 *Calculation methods for steadily loaded axial groove hydrodynamic journal bearings* (Engineering Science Data Unit).
5 **Barnard, D. P.** Oil flow in complete journal bearings. *Trans. SAE*, 1925, **20**(2), 66–81.
6 **Cole, J. A.** and **Hughes, C. J.** Oil flow and film extent in complete journal bearings. *Proc. Instn Mech. Engrs*, 1956, **107**, 499–510.
7 **Dowson, D., Hudson, J. D., Hunter, B.** and **March, C. N.** An experimental investigation of the thermal equilibrium of steadily loaded journal bearings. *Proc. Instn Mech. Engrs*, 1967, **181**(3B), 70–80.
8 **Andrisano, A. O.** An experimental investigation on the rotating journal surface temperature distribution in a full circular bearing. *J. Tribol.*, 1988, **110**(4), 638–645.
9 **Elrod, H. G.** and **Adams, M. L.** A computer program for cavitation and starvation problems. Proceedings of First Leeds–Lyon Symposium on *Tribology*, 1975, pp. 37–42 (Butterworths, London).
10 **Elrod, H. G.** A cavitation algorithm. *Trans. ASME, J. Lubric. Technol.*, 1981, **103**(3), 350–354.
11 **Dowson, D., Miranda, A. A. S.** and **Taylor, C. M.** Implementation of an algorithm enabling the determination of film rupture and reformation boundaries in a liquid film bearing. Proceedings of Tenth Leeds–Lyon Symposium on *Tribology*, 1984, pp. 60–70 (Butterworths, London).
12 **Clayton, G. A.** and **Taylor, C. M.** Design data for steadily loaded full central circumferential groove plain journal bearings. *Proc. Instn Mech. Engrs, Part C*, 1990, **204**(C1), 53–61.
13 **Brewe, D. E.** Theoretical modelling of the vapour cavitation in dynamically loaded journal bearings. *J. Tribol.*, 1986, **108**, 628–638.
14 **Woods, C. M.** The use of multi-grid techniques in the solution of Elrod's algorithm for dynamically loaded journal bearings. NASA report 180873, Lewis Research Center, 1988.
15 **McKee, S. A.** Oil flow in plain journal bearings. *Trans. ASME*, 1952, **74**, 841–848.
16 **Woolacott, R. G.** and **Macrae, D.** The performance at high speed of complete plain journal bearings with two axial oil-inlet grooves. NEL report 326, 1967.
17 **Miranda, A. A. S.** Oil flow, cavitation and film reformation in journal bearings, including an interactive computer-aided design study. PhD thesis, Department of Mechanical Engineering, University of Leeds, 1983.

APPENDIX

Definition of the parameters involved in equation (6):

$$X_1 = \bar{h}_j(1 - g_{i,j})$$

$$X_2 = g_{i,j}\bar{h}_j + \frac{g_{i,j}g_{i,j+1}}{2}(\bar{h}_{j+1} - \bar{h}_j)$$

$$X_3 = \frac{(\bar{h}_{j+1} + \bar{h}_j)^3 g_{i,j}}{\Delta\bar{x}_j} + \frac{(\bar{h}_j + \bar{h}_{j-1})^3 g_{i,j}}{\Delta\bar{x}_{j-1}}$$

$$X_4 = \frac{(\bar{h}_{j+1} + \bar{h}_j)^3 g_{i,j+1}(\Theta_{i,j+1} - 1)}{\Delta\bar{x}_j}$$

$$X_5 = \Theta_{i,j-1}\bar{h}_{j-1}(1 - g_{i,j-1}) + g_{i,j-1}\bar{h}_{j-1} + \frac{g_{i,j-1}g_{i,j}}{2}(\bar{h}_j - \bar{h}_{j-1})$$

$$X_6 = \frac{(\bar{h}_j + \bar{h}_{j-1})^3 g_{i,j-1}(\Theta_{i,j-1} - 1)}{\Delta\bar{x}_{j-1}}$$

$$X_7 = X_3 + X_4 + X_6$$

$$X_8 = X_5 - X_2$$

$$Y_1 = \bar{h}_j^3 g_{i,j}\left(\frac{1}{\Delta\bar{y}_i} + \frac{1}{\Delta\bar{y}_{i-1}}\right)$$

$$Y_2 = \left\{\frac{g_{i+1,j}(\Theta_{i+1,j} - 1)}{\Delta\bar{y}_i} + \frac{g_{i-1,j}(\Theta_{i-1,j} - 1)}{\Delta\bar{y}_{i-1}}\right\}\bar{h}_j^3$$

$$Y_3 = Y_1 + Y_2$$

$$\Delta\bar{x} = \frac{\Delta\bar{x}_j + \Delta\bar{x}_{j-1}}{2}$$

$$\Delta\bar{y} = \frac{\Delta\bar{y}_i + \Delta\bar{y}_{i-1}}{2}$$